

---

**From:** Dana Swift  
**To:** Webb Research, Gary DiBona  
**Date:** February 9, 2021  
**Subject:** Apex Pneumatic Bladder Air Entrapment & Darcy Loss

---

In December, 2020, UW discovered systematic pathology of the pneumatic system for almost all APEX purchased for the 2018-2019 period. In Fall, 2018, UW placed orders for 110 APEX (ie., all with Apf11 controllers) which were delivered in the first half of 2019. Of these, 104 APEX exhibit pathological loss of internal air post-deployment as evidenced by the steady decrease in internal barometric pressure. This represents a sudden drastic change when referenced against the 47 APEX with Apf11 controllers that were purchased for the previous (ie., 2017-2018) period.

The Apf11 controller is equipped with two pressure sensors; a 15psi sensor measures the absolute barometric pressure inside the float while a 30psi sensor is plumbed into the pneumatic system to measure absolute pressure inside the air bladder. Henceforth, I will refer to these as the barometric and pneumatic sensors, respectively. The Apf11 samples these sensors with a 12-bit AD converter which is then dithered (for historical reasons) to produce an 8-bit measurement.

Fig. 1 reveals that Apf11 floats purchased in 2017 exhibit normal behavior; only 2 of 47 floats (ie., 4%) suffered a pathological decrease in barometric pressure. The red curves show why we sounded the alarm; 104 of 110 floats (ie., 95%) show a steady decrease in barometric pressure which indicates that air is somehow leaving the system.

The ideal gas law (IGL) provides the relationship between the barometric pressure and the mass of air internal to the float:

$$\frac{p}{m} = \frac{R_s T}{V} \quad (1)$$

where ( $p$ ) is the barometric pressure, ( $m$ ) is the mass of air, ( $T$ ) is the air temperature (in Kelvins), ( $V$ ) is the volume of air, and ( $R_s$ ) is the specific gas constant. The barometric pressure is purposely measured at the end of the park phase where the thermal environment is very stable (ie.,  $T$  is constant) over the life of the float. Moreover, the pneumatic bladder is completely collapsed and the piston position remains stable (ie.,  $V$  is constant) over the life of the float. Since, the RHS of (1) is nearly constant over the life of the float then the mass of air is proportional to the barometric pressure

$$m = k \cdot p \quad (2)$$

where the proportionality constant is  $k = \frac{V}{R_s T}$ . The right-most axis in Fig 1 shows the fractional decrease of internal air mass corresponding to the decrease in barometric pressure. The pneumatic pathology causes the loss of 5%-20% of the initial mass of air in the float after only one year of operation.

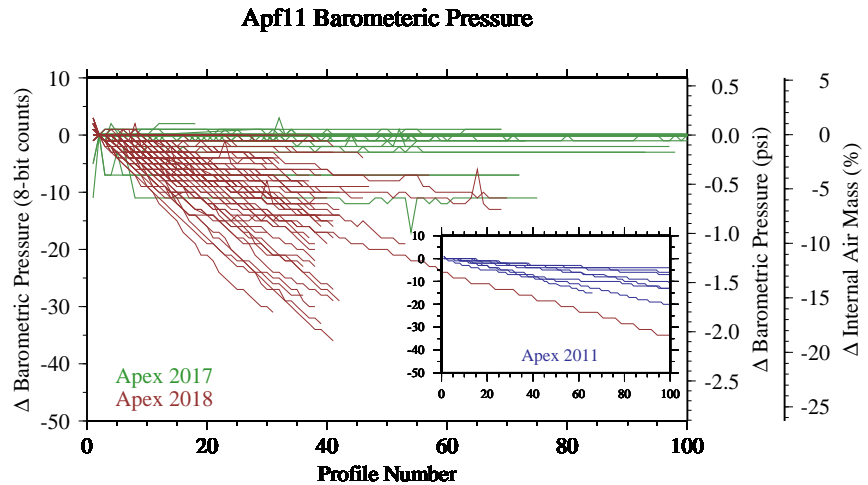


Figure 1: Green curves represent the reference batch of 47 APEX purchased in 2017; only 2 of 47 floats (ie., 4%) exhibit pathological decrease of barometric pressure. Red curves represents the 110 APEX purchased in 2018; 104 of 110 floats (ie., 95%) exhibit pathological decrease of barometric pressure. Historically, this pathology is uncommon although a smaller batch of floats from the 2011 purchase were similarly affected (see inset above).

(SWJ 29:18;eq(1))

(SWJ 20:18;eq(3))

## Symptoms of pneumatic pathology.

In addition to steady loss of air from inside the float, many other associated symptoms have been identified via analysis of engineering data from affected floats. The syndrome is associated with each of the symptoms below but not all affected floats exhibit all symptoms.

1. Loss of air from inside the float as previously discussed; this is the hallmark symptom.
2. The pneumatic bladder remains partially or completely deflated while at the surface despite repeated attempts to inflate. This was a secondary cause for poor telemetry and failure to acquire a GPS fix.
3. Premature termination of bladder inflation mechanism after only a few seconds of running the air pump.
4. Excess buoyancy that prevents the float from descending below the surface after the piston has been retracted to the previous park position.

These symptoms were used to formulate hypotheses about what caused the pathology; any hypothesis that could not explain all of these symptoms must be rejected. Three detailed case studies will help to eliminate many hypotheses.

### Case study: Apfld 18726

Float 18726 was selected because it provides the cleanest symptoms from which to build a conceptual model. It represents a canonical example that should be used to evaluate hypotheses that might explain the syndrome's cause. Fig. 2 very clearly illustrates the first three symptoms listed above.

During the first 12 profiles, both air-pump run-time and pneumatic pressure indicate successful bladder inflation. However, decreasing barometric pressure during these profiles indicates loss of internal air from the system.

Starting with profile 13, the pneumatic system is over-pressurized to  $\sim 190$  counts after running the air pump only 3 seconds. This indicates that only the Tygon tube connecting the air pump to the air bladder is being charged; the air bladder itself remains deflated. Simultaneously, barometric pressure levels off which indicates that no additional air is lost from the system. *This observation directly connects (and implicates) the pneumatic bladder with the loss of internal air; air loss happens only when bladder inflation is at least partially successful.*

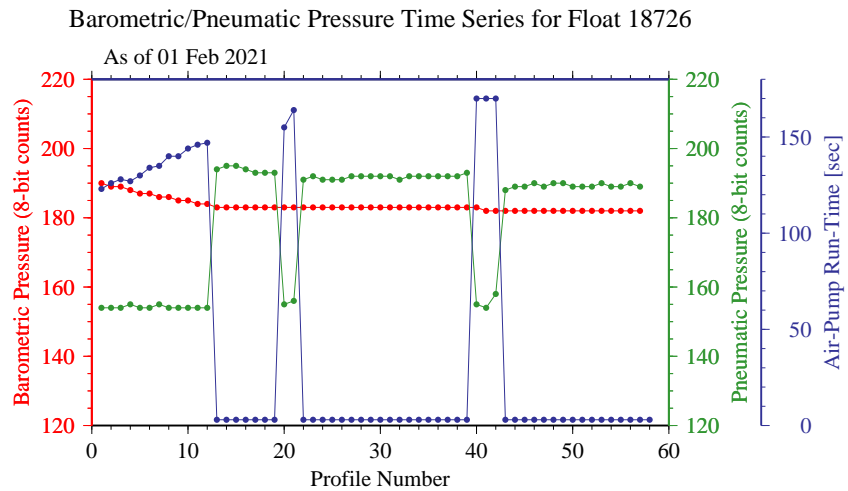


Figure 2: The red time-series represents barometric pressure measurements made at the end of the park phase. The green time-series represents the pneumatic pressure measured at the surface just after the air pump was shut-off. The blue time-series represents the length of time (in seconds) required for the air pump to charge the pneumatic system.

## Case study: Apfld 18510

Float 18510 exhibits all of the symptoms except that symptom (3) is intermittent and temporary. The intermittent and temporary character of symptom (3) is common amongst affected floats.

Fig. 3 shows strong and steady decreasing internal pressure. According to (2), the decrease of barometric pressure by 36 counts corresponds to the loss of 19% of its initial mass of air.

As the air pressure drops, the run-time of the air pump increases up to 225 seconds which is the maximum allowed by firmware.

Starting with profile 25, symptom (3) appears intermittently. During the telemetry phase, as many telemetry cycles are executed as necessary to upload all of the data. If a telemetry cycle ends with data still to be uploaded then the float sleeps for a few minutes before initiating another telemetry cycle.

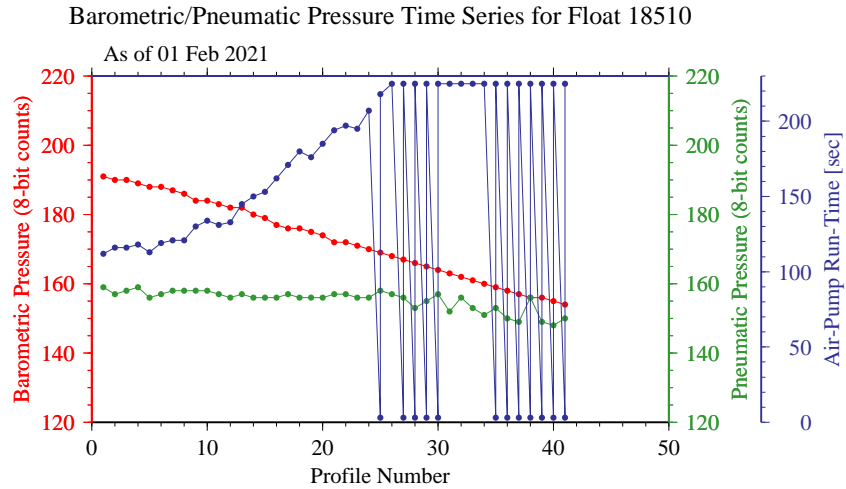


Figure 3: The blue curve shows that symptom (3) is intermittent and temporary. When the symptom occurs, bladder inflation is prematurely terminated only on the first telemetry cycle; the second telemetry cycle is always successful.

All of the profiles in Fig. 3 that exhibit two different run-times required multiple telemetry cycles. All experienced the same pattern of behavior. During the first telemetry cycle, the air pump ran for only 3 seconds after which the pneumatic pressure measured approximately 190 8-bit counts. This far exceeds the cut-off threshold of 154 counts and so indicates that something prevented air from inflating the air bladder. However, this condition is temporary because bladder inflation is successful on the second telemetry cycle.

This float also suffers from the occasional inability to descend from the surface after the telemetry phase is complete. For example, the engineering log<sup>1</sup> for profile 26 includes the following snippet that indicates that the float remained at the surface for more than 120 hours after the piston had been retracted to the previous profile's park position:

```
(Aug 15 2020 15:44:00,      1 sec) DescentInit()      Deep profile 26 initiated at mission-time 860259sec.
(Aug 15 2020 15:44:01,      2 sec) DescentInit()      Surface pressure: 0.2dbars.
(Aug 15 2020 15:44:13,     14 sec) DescentInit()      Pneumatic humidity: 1052(6.8%) -> 1101(8.2%)
(Aug 15 2020 15:44:13,     14 sec) PistonMoveAbsWT0()  186->081 185 184 183 182 181 [snippage...]
                                083 082 081 [496sec, 14.7Volts, 0.135Amps, CPT:496sec]
(Aug 15 2020 15:52:38,     519 sec) Descent()      Pressure: 0.4
(Aug 15 2020 16:43:59,    3600 sec) Descent()      Pressure: 0.3
(Aug 15 2020 17:43:59,    7200 sec) Descent()      Pressure: 0.5
(Aug 15 2020 18:43:59,   10800 sec) Descent()      Pressure: 0.3
(Aug 15 2020 19:43:59,   14400 sec) Descent()      Pressure: 0.4
[snippage...]
(Aug 20 2020 15:44:04,   432005 sec) Park()      ParkPOutOfBand[-3, 0.4 dbars]: retract piston.
(Aug 20 2020 15:44:04,   432005 sec) PistonMoveAbsWT0()  043->042 042 [6sec, 15.0Volts, 0.147Amps, CPT:695sec]
(Aug 20 2020 19:44:04,   446405 sec) Park()      ParkPOutOfBand[3, 1609.9 dbars]: extend piston.
```

<sup>1</sup><http://runt.ocean.washington.edu/argo/data/18510/18510.026.log>

When the float finally did sink, it descended all the way down to 1609 dbars which is much deeper than the park pressure (ie., 1000 dbars). This is very strong evidence that air remains in the bladder or hydraulic system. In fact, this closely matches the behavior of floats with the N<sub>2</sub> compressesee, if the compensator hyper-retraction feature is not used.

## Case study: ApfId 18340

Float 18340 was selected because it was deployed, suffered pneumatic pathology, and was recovered after 69 profiles. Diagnostically, this float is the most important because we can investigate its pathology in the lab.

Fig. 4 shows that this float was relatively mildly affected by the syndrome despite exhibiting three of the four symptoms listed previously. The barometric pressure dropped from 193 (on profile 2) down to 180 which indicates a loss of 7% of its air mass. The float remained at the surface for the entirety of profile 65 indicating that enough air was trapped in the air bladder or hydraulic system to prevent its descent. Warmer temperatures at the surface explain the upward blip in the barometric pressure during profile 65. Two instances of sticky-bladder occurred during profiles 34 & 40 that initially prevented bladder inflation. In both cases, the bladders were successfully inflated on subsequent telemetry cycles.

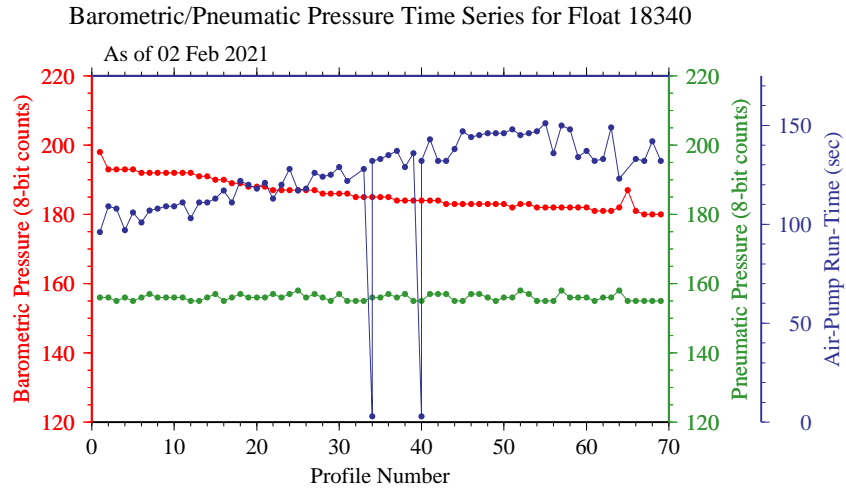


Figure 4: Despite exhibiting relatively mild pathology, float 18340 was crucial to discovering the syndrome’s cause.

## Laboratory diagnostics of ApfId 18340.

### Overnight bladder test.

Prior to any disassembly, we performed one of our standard tests that we refer to as the “Overnight Bladder Test”. The purpose of this test is to detect loss of air from the inflated bladder. The air bladder was inflated using the firmware’s AirSystem() routine just as is used during its mission. The solenoid valve is closed and the bladder is inflated with a one-second-on/one-second-off pulse of the air pump until the pressure exceeds its specified threshold for three consecutive pulses. The float was secured in a vertical orientation and induced into a “frozen” state to prevent firmware from executing any further operations. The float remained undisturbed for a 24-hour period after which the air pressure is measured using the Apf11’s pneumatic pressure sensor. It is normal for the pneumatic pressure to drop by 3-4 counts over the 24-hour period due to relaxation of the plastic cowling. The float passed this test and so any hypotheses regarding air loss that rely on pin-holes or weld failure are excluded since air loss far more than 3-4 counts are associated with this pathology. Similarly, this test excludes a low-pressure air leak past the air/oil gasket seal into the hydraulic system.

## Ballasting procedure as a diagnostic test.

The float was opened and inspected to ensure that nothing pinched, kinked, blocked, or compressed the Tygon tube that connected the air pump to the air bladder. General function testing was performed to confirm that the pneumatic system operated as expected. The float was internally reconfigured so that the float could be ballasted in fresh water in our large pressure test vessel (PTV). After reassembly and preparations for ballasting were finished, the air bladder was visually inspected to ensure that it was completely deflated.

We discovered that it was not possible to ballast the float using our normal procedure. In fact, the float behaved similarly to one equipped with an  $N_2$ -compressor. With the float neutrally buoyant while suspending 23 inches of chain, we increased the water pressure in the PTV. As the water pressure increased, the buoyancy of the float decreased until the float rested on the bottom of the PTV.

This observation is clear evidence for air in the hydraulic system.

## Noninvasive measurement of air volume in the hydraulic system.

Fig. 5 shows UW's small PTV that was custom designed to subject the lower end-cap assembly to the full range of water pressure while simultaneously allowing access to the inside of the float. It includes provision to bleed air at its highest point so that the internal volume is completely filled with water.

The float was mounted in the PTV and its solenoid valve opened to allow the air bladder to deflate. The PTV was initially charged with normal city water pressure (ie.,  $\sim 60$  psig) before closing a valve to render a closed system that could be further pressurized using the float's hydraulic pump. The Apf11 was used to control and measure the piston position. The water pressure increased as the piston was extended and the PTV's gauge was used to measure pressure.

The volume displacement (ie., piston position) was measured over the range of pressures from approximately  $60 \leftrightarrow 2500$  psig. The range was traversed four times in patterns of increasing and then decreasing pressure. The green triangles in Fig. 6 represent 44 measurements of the volume displacement (ie., piston position) as a function of pressure.

The compressible volume includes distinct elements that are solid, liquid, or gas as represented by the PTV vessel, oil/water, or air, respectively. The compressibility of the solid & liquids are approximately constant but the compressibility of the air is very nonlinear.



Figure 5: This pressure test vessel (PTV) was custom designed to subject the lower end-cap assembly to high pressure water while simultaneously allowing access to the inside of the float.

The ideal gas law (IGL) provides the relationship between pressure (P) and volume ( $V_a$ ) of the air:

$$PV_a = nRT = k \text{ (constant)} \quad (3)$$

where ( $R = 8.314 \text{ m}^3 \cdot \text{Pa} \cdot \text{K}^{-1} \cdot \text{mol}^{-1}$ ) is the ideal gas constant, (n) is the moles of air, and (T) is the temperature (in Kelvins). The time required to cycle the pressure up and back down is less than 45 minutes and so dissolution of air into the oil can be neglected. Since both the temperature and the moles of air remain approximately constant then the RHS of (3) is constant:  $k = nRT$ . Therefore, the volume of air at any given pressure is

$$V_a = \frac{k}{P} \quad (4)$$

Volume displacement by the piston must be accommodated while simultaneously satisfying the IGL. Initially, the piston position is ( $c_o$ ) and the pressure is ( $P_o$ ). The total volume displaced when the piston position is ( $c$ ) is given by  $\frac{dV}{dc}(c - c_o)$  where  $\frac{dV}{dc} = 1.13 \frac{\text{ml}}{\text{count}}$ . The volume displacement is partitioned between the solid/liquid and gas phases according to the following expression:

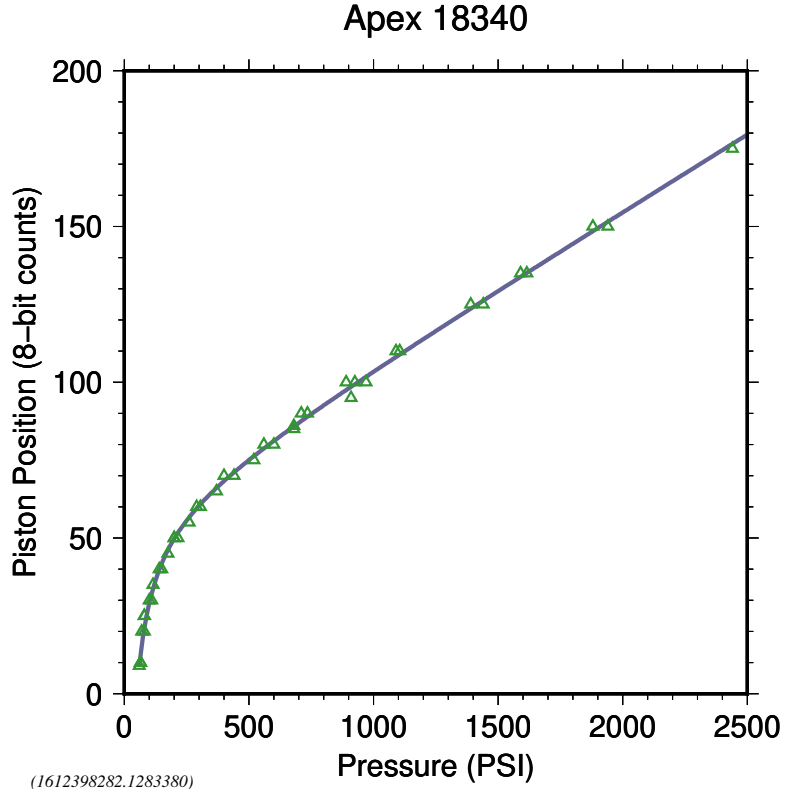


Figure 6: The green triangles represent 44 measurements of the volume displacement (ie., piston position) as a function of pressure. The blue curve represents a weighted least-squares best-fit to a mathematical model of associated physics. The nonlinear character of the P-V curve is the hallmark signature of the presence of air in the hydraulic system. Moreover, the curve's concavity quantitatively encodes the volume of trapped air.

$$\frac{dV}{dc}(c - c_o) = \left. \frac{\partial V}{\partial P} \right|_{\ell} (P - P_o) + k \left( \frac{1}{P} - \frac{1}{P_o} \right) \quad (5)$$

where  $\left( \left. \frac{\partial V}{\partial P} \right|_{\ell} \right)$  is a constant associated with compressibility of the solid/liquid phases. The last term on the RHS represents the volume change of the air bubble when the pressure increases from  $P_o$  to  $P$ . Note that for the initial condition ( $c = c_o, P = P_o$ ) then all three terms in (5) are equal to zero.

All of the quantities in (5) are directly measured except for the two unknowns:  $\left. \frac{\partial V}{\partial P} \right|_{\ell}$  and k. The 44 measurements were used to solve for these two unknowns using a standard weighted least-squares method. The blue curve in Fig. 6 represents the function,  $c(P)$ , that is a best-fit to the 44 measurements. The function is derived by solving (5) for (c) and considering all quantities, except (P), to be known parameters. The variable (P) determines the volume displacement and its partitioning according to (5).

The correctness of the model physic seems evident by the closeness of the blue curve to the green measurements in Fig. 6, Having formulated the model, it is now possible to compute the volume of the air bubble to be  $V_a = 149 \text{ ml}$  at atmospheric pressure.

## Direct measurement of air volume in the hydraulic system.

Having made every noninvasive effort to show that the hydraulic system contained a trapped air bubble, we decided to try to actually extract the air bubble from the hydraulic system; nothing eliminates uncertainty as effectively as direct proof. A video of the extraction process is available by pointing your browser here: <http://runt.ocean.washington.edu/swift/AirRecoveryMethodFromHydraulicSystem.mp4>

The cowling was removed and the float was secured in a vertical orientation. The air bladder was inflated until it resembled a quasi-sphere with the objective of forming the oil bladder into the shape of an inverted bowl. Next, the Apf11 was used to pump 150ml of oil into the oil bladder so that any air that was in the oil bladder would rise to the top of the inverted bowl to where the oil ports could collect it. The piston was fully retracted to draw the air back into the cylinder. This process was repeated to ensure that all of the air was transferred from the oil bladder into the cylinder. The chassis was separated from the lower end-cap assembly and the hydraulic line was disconnected from the its fitting. A vertical orientation was maintained so that the air bubble would remain at the top of the cylinder.

Tygon tubing was connected from an inverted jar to the oil line as shown in Fig. 7. A second Tygon tube would empty water into a beaker so that the volume of displaced water could be measured. The Tygon tubes and inverted jar were completely full of water. As shown in Fig. 7, the float chassis was inverted and clamped so that the air bubble would rise to the top of the inverted cylinder. The Apf11 was used to extend the piston to push the air bubble out of the cylinder, through the tygon tube, and into the jar. The air bubbles floated to the top of the jar while the displaced water was collected in the beaker to be measured. The hydraulic pump was allowed to run until all of the air was discharged from the cylinder; the volume of air was measured to be 110ml.

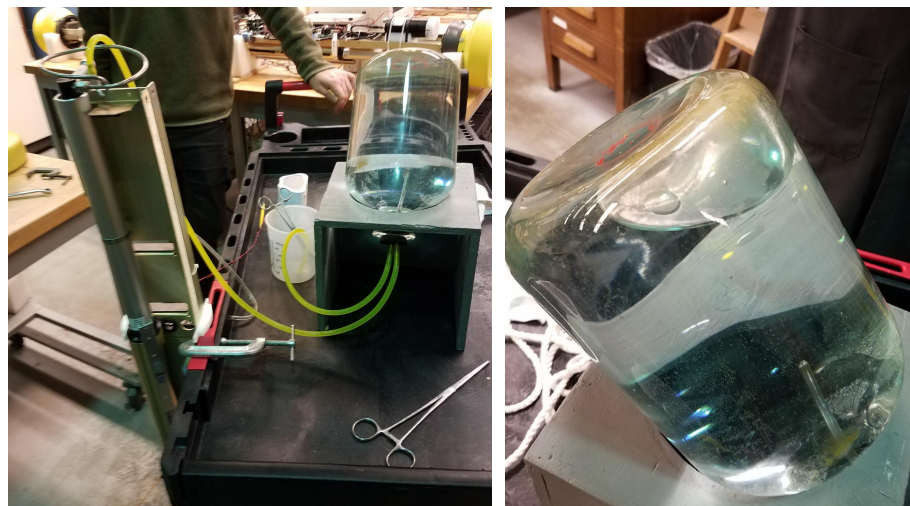


Figure 7: (left) The trapped air bubble was extracted using an inverted jar filled with water and a beaker to measure the volume of water displaced by the recovered air bubble. (right) The large (110ml) air bubble is shown in the top of the inverted jar after the extraction process was complete.

## Discrepancy: Volume of air measured by different methods.

The large air bubble shown in the top of the jar in Fig. 7 displaced 110ml of water into the beaker. This represents only 74% of the 149ml that was measured by the noninvasive method described in the previous section. The source of this discrepancy is unknown but possibilities include that not all of the air was recovered by the extraction process or perhaps the noninvasive method over-estimated the volume if not all of the air was bled from the PTV.

## Destructive examination of the pneumatic bladder.

The air bladder from ApfId 18340 (WrcId 8686) was sectioned and examined. For comparison purposes, ApfId 17762 (WrcId 8369) was selected as a reference because its air bladder originated from a previous batch of floats that were unaffected by the pathology. Figures 8 and 9 show photographs of the mating surfaces of the outer and inner walls of the air bladders for the affected and reference floats, respectively. Based on a qualitative visual and tactile examination, both surfaces of the reference bladder (Fig. 9) are characterized by linear striations and a rough appearance. As will be described later, both of these features are crucial to prevent air from being trapped in the bladder. In contrast, the mating surfaces of the affected float (Fig. 8) are much smoother with striations almost completely absent on the inner wall.



Figure 8: **ApfId 18340 Bladder Section:** (left) The inner surface of the outer wall of the air bladder is marked by linear striations with a median transverse roughness (Ra) measured to be  $16\mu\text{m}$ . (right) The inner surface of the inner wall of the air bladder is smooth and shiny with only a few striations. The median roughness was measured to be  $12\mu\text{m}$ .

The mating surfaces of the affected and reference air bladders were measured using a roughness gauge. Table 1 lists the measurements for each surface in increasing order of roughness (Ra); the median values are displayed in bold. The quantitative measurements confirm the qualitative observation that the roughness of the reference bladder is much higher than the affected bladder. This is particularly true for the inner wall where the roughness of the reference bladder is 3.4 times than the affected bladder. These measurements will form the basis for a conceptual model of the pathology.

The durometer of the reference bladder was measured to be 82 on the Shore A scale. The affected bladder measured 77.

ApfId 18340 (WrcId 8686)		ApfId 17762 (WrcId 8369)	
Outer Wall	Inner Wall	Outer Wall	Inner Wall
$\mu\text{m}$	$\mu\text{m}$	$\mu\text{m}$	$\mu\text{m}$
15.15	10.42	24.64	31.98
15.19	10.74	25.02	37.08
<b>15.97</b>	<b>11.81</b>	<b>26.52</b>	<b>39.63</b>
18.85	16.26	40.54	48.82
20.43	16.79	48.23	48.95

Table 1: The roughness (Ra) of the mating surfaces for air bladders from floats 18340 and 17762 were measured in five places transverse to the striations. The median values (in bold) demonstrate that the roughness of the reference bladder is 1.7 to 3.4 times higher than the affected bladder.

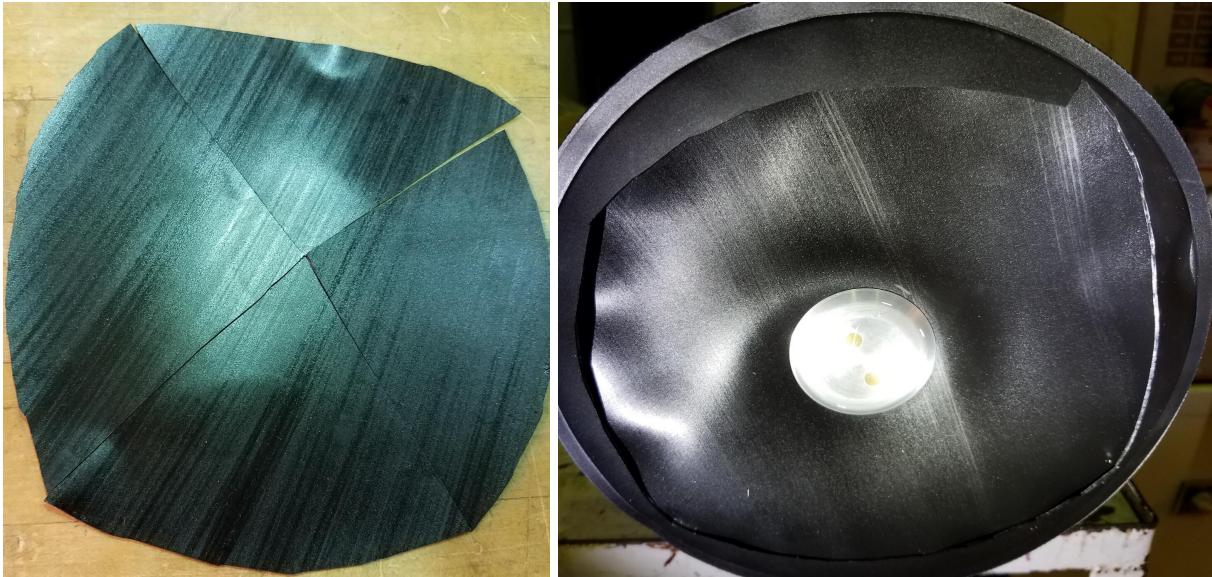


Figure 9: **Apfld 17762 Bladder Section:** (left) The inner surface of the outer wall of the air bladder is marked by linear striations with a median transverse roughness ( $R_a$ ) measured to be  $27\mu\text{m}$ . (right) The inner surface of the inner wall of the air bladder has distinct linear striations and a median roughness  $40\mu\text{m}$ .

## Air entrapment and Darcy loss.

The evidence supports the conclusion that the loss of air from floats is caused when air remains trapped in the air bladder after the float has submerged from the surface. As the float descends, the pressurized air forces a Darcy flow through both bladder walls into the ocean and the oil bladder. The resulting loss of air is measured as decreasing air pressure internal to the float. The cycle is repeated with each profile and continues until the air pump can no longer develop enough pressure to inflate the air bladder.

## Proposed solution: Surface roughness and durometer.

Darcy flows through anisotropic media provide a solid conceptual framework with which the air entrapment problem can be understood and solved. Under high water pressure, the collapsed bladder constitutes a porous substrate through which air will flow in response to a pressure gradient. To prevent air from being trapped, it is crucial that the radial porosity at the wall-interface be much larger than the porosity of the bladder material. If the radial porosity can be managed as quality control issue then the rate of Darcy flow toward the center fitting will be high enough to prevent Darcy loss of air into the ocean or hydraulic system.

Fig. 10 shows a cartoon model of an area near the center fitting of the deflated air bladder and hint that the striations form channels through which air can flow in response to a pressure gradient. Fig. 10L depicts a bladder where the inner wall lacks striations (ie., float 18340). Most striations do not intersect the center fitting and so trapped air can not flow back inside the float. On the other hand, Fig. 10R depicts a bladder with obliquely-intersecting striations on both walls. The cross-hatched pattern of intersecting channels facilitates air flow radially inward toward the center fitting from anywhere within the bladder. The enhanced radial Darcy flow allows the air bladder to completely deflate and so prevents air loss from the system.

The reference bladder shown in Fig. 9 and its surface roughness as measured in Table 1 will be used to

specify bladders with adequate radial porosity.

Table 1 makes clear that there is a distinct measurable difference in the surface roughness (measured transverse to the striations) of the reference bladder in comparison to the bladder from float 18340. Based on these measurements, we will propose that the presence of striations with a minimum median surface roughness ( $R_a$ ) of  $25\mu\text{m}$  be required of the sheets of material used to make the bladders. The striations on each wall of the air bladder should be obliquely oriented and facing each other. In addition, the minimum durometer of the material should be 80 on the Shore A scale to prevent the channels from collapsing under pressure.

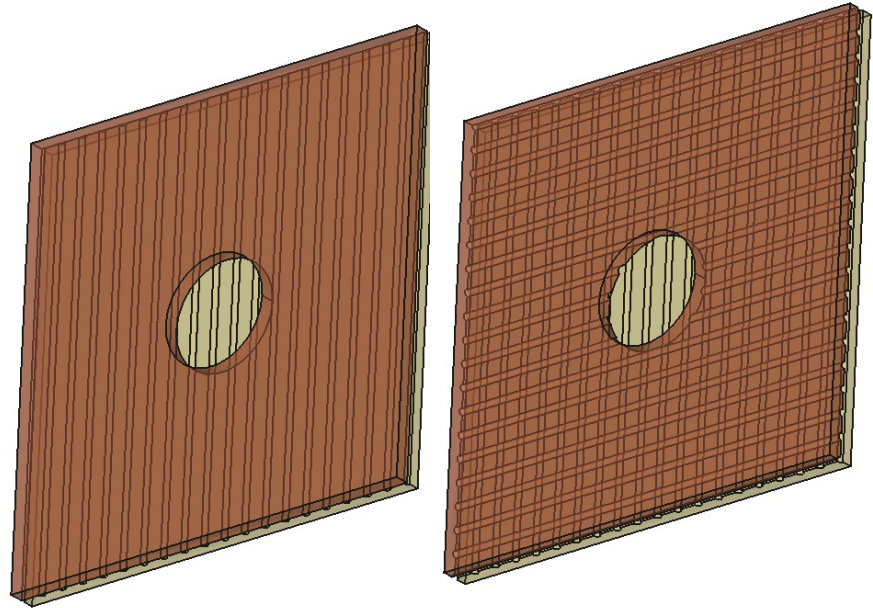


Figure 10: This cartoon model of the portion of air bladder near the fitting reveals the importance of striations on the surfaces of both walls. (*left*) For most sectors, striations on only one surface prevent access to a channel that intersects the center fitting. (*right*) Obliquely oriented striations on both walls facilitate channels that connect the center fitting to anywhere in the bladder.

### Bladder stiction.

The premature deactivation of the air pump (Page 2, Symptom 3) experienced by some floats remains poorly understood but seems clearly associated with the same pathology that causes air loss. We have been unable to replicate the problem in the lab but the evidence supports a hypothesis that the two walls of the bladder become fused together. We've been referring to this as "stiction" despite that static friction is not involved. We wonder if the bladder material requires a curing process during bladder fabrication. If so, then perhaps the bladders were undercooked which might leave them susceptible to fusing together under the extreme and prolonged pressures experienced during deployment. The total load on the bladder exceeds 87000 lbs for days followed by up to 174000 lbs for 10 hours, or so.

Although stiction seems the most obvious candidate, anything that would have the effect of preventing air from entering the bladder would produce the same symptoms. For example, if the durometer is too low, it's also possible that such extreme pressure might extrude some of the bladder material into the air-ports of the center fitting. Plugging these ports would cause the premature deactivation of the air pump. Although float 18340 experienced this symptom only twice, the section bladder clearly shows permanent impressions of the center fitting and all six air-ports (see Fig. 8). Perhaps the bladder on float 18726 has lower durometer that allowed bladder material to extrude into and plug the ports.